INVESTIGATION OF CHARACTERISTICS OF PRESSURE WAVES GENERATED IN WATER FILLED TANKS IMPACTED BY HIGH-VELOCITY PROJECTILES

by Francis S. Stepka, C. Robert Morse, and Robert P. Dengler

Lewis Research Center
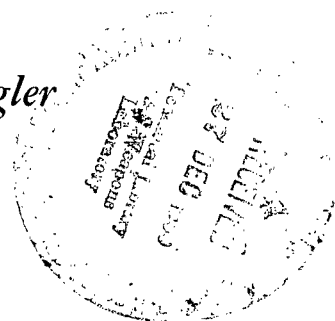*Cleveland, Ohio*

INVESTIGATION OF CHARACTERISTICS OF PRESSURE

WAVES GENERATED IN WATER FILLED TANKS

IMPACTED BY HIGH-VELOCITY PROJECTILES

By Francis S. Stepka, C. Robert Morse, and Robert P. Dengler

Lewis Research Center
Cleveland, Ohio

INVESTIGATION OF CHARACTERISTICS OF PRESSURE WAVES GENERATED

IN WATER FILLED TANKS IMPACTED BY HIGH-VELOCITY PROJECTILES

by Francis S. Stepka, C. Robert Morse, and Robert P. Dengler

Lewis Research Center

SUMMARY

A high-speed rifle and a light-gas gun were used to accelerate projectiles for impact into transparent water filled tanks over a range of velocities from 1.31 to 6.40 kilometers per second. The projectiles were solid spheres or cylinders of either copper, steel, Nylon, aluminum, or tungsten carbide ranging in diameter from 1.59 to 5.56 millimeters (1/16 to 7/32 in.).

The wave front shape, the progress of the wave front as a function of time, and the intensity of liquid pressures induced as a result of the projectile impact were determined for the various impact conditions with a high-speed, continuous-writing, framing camera. Measurements and analytical predictions of the deceleration of the projectile in the liquid were also obtained to help relate the change of projectile kinetic energy to the characteristics of the pressure wave generated.

The projectile impacts, which resulted in a rapid transfer of energy to the liquid, produced essentially a "point source" energy release and resulted in an expanding, spherically shaped, pressure wave front that emanated from the point of impact. Extremely high pressures were generated in the liquid close to the point of impact, but these pressures decayed rapidly as the wave front propagated away from the point of impact. The progress of the wave front during the period of intense pressures was found to be proportional to time to about the 0.8 power.

If simplifying assumptions are utilized and only drag forces on the projectile are considered, analytical predictions of the energy lost by spherical projectiles at any time after impact agree well with experimental data.

INTRODUCTION

The hazard of meteoroid impact into liquid propellant tanks are of particular concern because an impact of sufficient energy could not only puncture the tank but could result in a catastrophic bursting or tearing of the tank wall.

A preliminary experimental study (ref. 1) evaluated some of the factors

responsible for fracture of liquid-filled tanks impacted by high-speed projectiles. The reference indicated that the shock pressures generated in the contained liquid by the decelerating projectile was the primary factor effecting wall fracture. Although some insight into the characteristics of the shock wave was obtained, the data presented were limited to impacts by the same size and shape projectiles and at relatively low velocities (<2.3 km/sec).

Knowledge of the shape and rate of propagation of the shock front in the impacted liquid is necessary for the prediction of the characteristics and the magnitudes of the pressures induced in the liquid. Relating these factors to projectile impact condition is also necessary to analyze the meteoroid impact and tank wall fracture problem. At the initiation of this investigation analyses, such as references 2 and 3, of shock wave front propagation in solid targets resulting from projectile impact were available; however, no known analysis of the pressure pulse generated in liquids from projectile impacts existed. The analyses of references 2 and 3 are based on blast wave theory and assume that the impacting projectile essentially produced an intense "point source" of energy that resulted in a shock front with a hemispherical shape. The results of these analyses indicated that the progress of the shock front was proportional to time to an exponent. The exponent, dependent on whether a conservation of momentum or kinetic energy was assumed, ranged from 0.25 to 0.4. A more recent analysis (ref. 4) indicates that the pressure front progress under actual impact conditions, initially, and particularly during the later stages of the cratering process may not meet the conditions of extremely high energy loading assumed in reference 3. The analysis indicates that after a constant speed phase of the shock front during which the projectile is destroyed, the shock progress is proportional to time to the 0.4 to 1.0 power depending on the energy of the impact. Although the latter analysis agrees reasonably well with experimental data of impacts into solids, the applicability of the cited analyses to impacted liquids was not known.

Concurrently with the investigation reported herein two analyses (refs. 5 and 6) were made of the progress of the shock fronts in water impacted by projectiles. Both of these analyses were generally successful in the prediction of the progress of the front with time. Reference 5 was restricted to predicting the complete wave progress for individual impacts by using some of the data of the experimental wave progress for these particular impacts to evaluate constants required in the analysis. The equation of shock wave progress with time presented in reference 6, however, has more general application. It correlated the wave front progress with available experimental data by using the impact kinetic energy of the projectile. The experimental data used in both references were primarily limited to low-velocity projectiles and projectiles of constant diameter.

The purposes of the investigation reported herein, therefore were as follows:

(1) Determine the shape, progress with time, and pressures of the shock front generated in water filled tanks impacted by projectiles of various sizes, shapes, and materials over a range of impact velocities

(2) Compare the shock front characteristics in a liquid with those in solids and also with those assumed or predicted by the analyses discussed

(3) Measure the movement and deceleration of the projectile after impact into the liquid

(4) Relate the pressures generated in the liquid to projectile impact conditions (such as velocity, material, size, and shape) and to projectile deceleration in the liquid

Experiments were conducted by impacting water filled transparent plastic tanks with spherical and cylindrical projectiles of various materials. The projectiles varied in diameter from 1.59 to 5.56 millimeters (1/16 to 7/32 in.) and were accelerated to impact velocities between 1.31 and 6.40 kilometers per second by either a high-speed rifle or a light-gas gun. The projectile materials were aluminum, Nylon, copper, steel, and tungsten carbide. A high-speed framing camera was used to obtain shadowgraphs of the impact process at framing rates up to 500 000 frames per second to study the characteristics of shock waves produced in the liquid.

APPARATUS AND PROCEDURE

The test apparatus consisted of projectile accelerators, test tanks, and associated instrumentation for investigating the characteristics of the pressure waves generated in water from impacts by projectiles of various materials and shapes.

Projectile Accelerators

Low velocity (below 2.3 km/sec). - A 220 Swift rifle was used to accelerate projectiles for the low-velocity impacts. The rifle was mounted on a stand (fig. 1) and located about 2 meters from the target tank. An electrical solenoid was used to operate the trigger mechanism so that the rifle could be fired remotely. Impact tests were made over a range of projectile velocities (up to
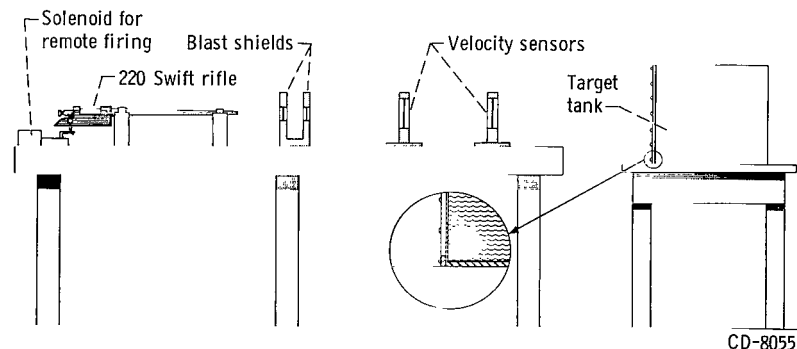

Figure 1. - Schematic of low-velocity projectile accelerator.

2.3 km/sec) by handloading cartridges with specific amounts of rifle powder.

High velocity (above 2.7 km/sec). - An accelerated-reservoir light-gas gun, similar to that described in reference 7, was used to accelerate projectiles for the high-velocity impacts. Velocities obtained with the projectile accelerator used ranged from about 2.74 to 6.40 kilometers per second. Figure 2 shows a schematic drawing of the gun facility; the main components of the gun are the powder chamber, a pump tube, a high-pressure coupling, and a launch tube 1.22 meters (48 in.) long, which has a bore diameter of 5.59 millimeters (0.22 in.).

Projectiles

The projectiles used for the impact test consisted of solid spheres ranging in size from 1.59 to 5.56 millimeters (1/16 to 7/32 in.) in diameter, and solid cylinders 5.56 millimeters (7/32 in.) in diameter with ratios of length to diameter from 1 to 2.7. Projectile materials were Nylon, aluminum, copper,
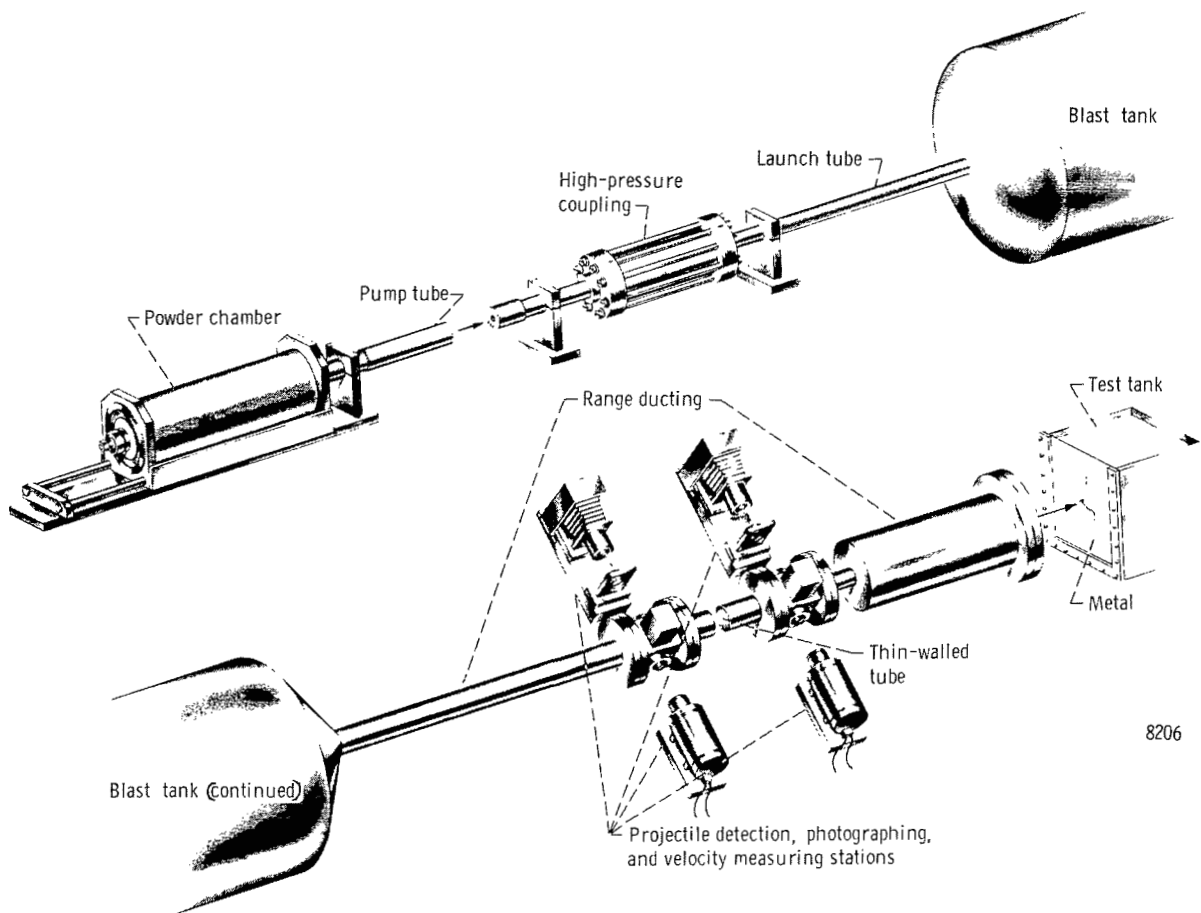

Figure 2. - Schematic of high-velocity projectile accelerator.

4

steel, and tungsten carbide; the particle mass ranged from 0.016 to 2.89 grams. Specific details are given in table I.

Sabot-Projectile Separation Devices

For those tests involving projectiles of diameters smaller than that of the launch tube bore, it was necessary to use a sabot. The sabot (see inset of fig. 3(a)) was a Lexan or Nylon rod 5.56 millimeters (7/32 in.) in diameter by 5.56 millimeters (7/32 in.) long that provided a gas seal and held the projectile during its travel in the launch tube. After exiting from the launch tube, the sabot was separated from the projectile and removed from the projectile flight path so that only the projectile impacted the target tank. Considerable difficulty was experienced in attaining this objective. Of the many schemes or separator devices experimented with during this investigation, the three devices shown in figure 3 were found to be most successful. All devices were essentially extensions of the launch tube and incorporated the principle of high drag and/or physical restrictions for separating the sabot from the projectile. The device in figure 3(a) used a cast paraffin cylinder with a central tapered hole to provide the drag and physical restriction to the sabot and permit the projectile to continue in its flight path to the target tank. The other two devices utilized polyethylene rings to provide the physical restriction to the sabot. The device of figure 3(b) used a series of 6.35-millimeter-thick (1/4 in.) rings. Each succeeding ring has a smaller diameter, the final hole size being 4.76 millimeters (3/16 in.) in diameter. The device of figure 3(c)

TABLE I. - SUMMARY OF HIGH-VELOCITY PROJECTILE IMPACTS INTO WATER-FILLED TANKS

Test number	Projectile					Impact		Impact energy, J	Tank wall configuration[a]
	Diameter, mm		Material	Shape	Mass, g	Velocity, km/sec	Mach number		
1	5.56	(7/32 in.)	Aluminum	Sphere	0.251	1.89	1.29	447	1.27-cm-diam. tube into tank center
2	3.175	(1/8 in.)	Steel	Sphere	.130	2.64	1.80	454	Solid, at 45° to direction of impact
3	1.59	(1/16 in.)	Steel	Sphere	.016	5.35	3.65	232	Prepunched, 7.62 cm hole
4	3.175	(1/8 in.)	Aluminum	Sphere	.047	5.27	3.60	649	Prepunched, 7.62 cm hole
5	5.56	(7/32 in.)	Aluminum	Sphere	.251	2.32	1.58	672	Prepunched, 1.27 cm hole
6	5.56	(7/32 in.)	Copper	Cylinder (5.56 mm long)	.972	3.96	2.70	7624	Prepunched, 5.08 cm hole
7	5.56	(7.32 in.)	Steel	Cylinder (5.56 mm long)	.907	4.27	2.91	8254	Prepunched, 5.08 cm hole
8	3.175	(1/8 in.)	Steel	Sphere	.130	4.27	2.91	1185	Prepunched, 7.62 cm hole
9	5.56	(7/32 in.)	Aluminum	Sphere	.251	1.90	1.30	451	Prepunched, 1.27 cm hole
10	5.56	(7/32 in.)	Tungsten Carbide	Sphere	1.345	~1.80	1.23	2173	Prepunched, 1.27 cm hole
11	5.56	(7/32 in.)	Copper	Cylinder (15.24 mm long)	2.890	~1.31	.89	2483	Prepunched, 1.27 cm hole
12	5.56	(7/32 in.)	Aluminum	Sphere	.251	~1.83	1.25	419	Solid
13	3.175	(1/8 in.)	Steel	Sphere	.130	3.75	2.56	915	Solid
14	3.175	(1/8 in.)	Steel	Sphere	.130	3.20	2.18	667	Solid
15	5.56	(7/32 in.)	Nylon	Cylinder (5.56 mm long)	.227	6.40	4.37	4640	Solid
16	5.56	(7/32 in.)	Steel	Sphere	.699	1.87	1.28	1218	Prepunched, 1.27 cm hole
17	5.56	(7/32 in.)	Aluminum	Sphere	.251	1.67	1.14	350	Prepunched, 1.27 cm hole

[a]All impacts were normal to the tank wall except for test no. 2.

5

used just one ring 12.7 millimeters (1/2 in.) in thickness with a hole size of 4.76 millimeters (3/16 in.). Configuration 3(c) was most successful and was used for the majority of the tests in this investigation.

Test Tanks

The test tanks used for the impact tests were fabricated from transparent plastic 12.7 millimeters (1/2 in.) or 19.05 millimeters (3/4 in.) thick. The tanks were rectangular in shape, open at the top, and had one removable and replaceable wall into which impact was made. A photograph of one of the tanks (after impact) is shown in figure 4. In this investigation the removable wall was made from 7075-T6 aluminum sheet 0.794 millimeter (1/32 in.) thick. The sheet was secured to the transparent walls by a contact cement or a clamping frame. Two sizes of test tanks were used. One was 61 centimeters (24 in.) square by 30.5 centimeters (12 in.) deep; the other was a cube 30.5 centimeters (12 in.) on a side. For the larger tank the wall to be impacted and penetrated was 61 centimeters square.

The tanks were filled with water and projectiles were impacted into the aluminum walls which were either solid or prepunched. Before testing, the

Enlarged section
of sabot

—Drilled hole (Depth
to submerge pro-
jectile about one-
half diam.)

—Insert tapered hole,
4.76-mm diam. at exit

Relief holes
for driving gas

Relief holes for
expanding insert

(a) Cast tapered insert. Insert material, paraffin.

—Polyethylene rings

—Exit hole,
4.76-mm diam.

(b) Multiple polyethylene rings.

12.7-mm-thick polyethylene ring
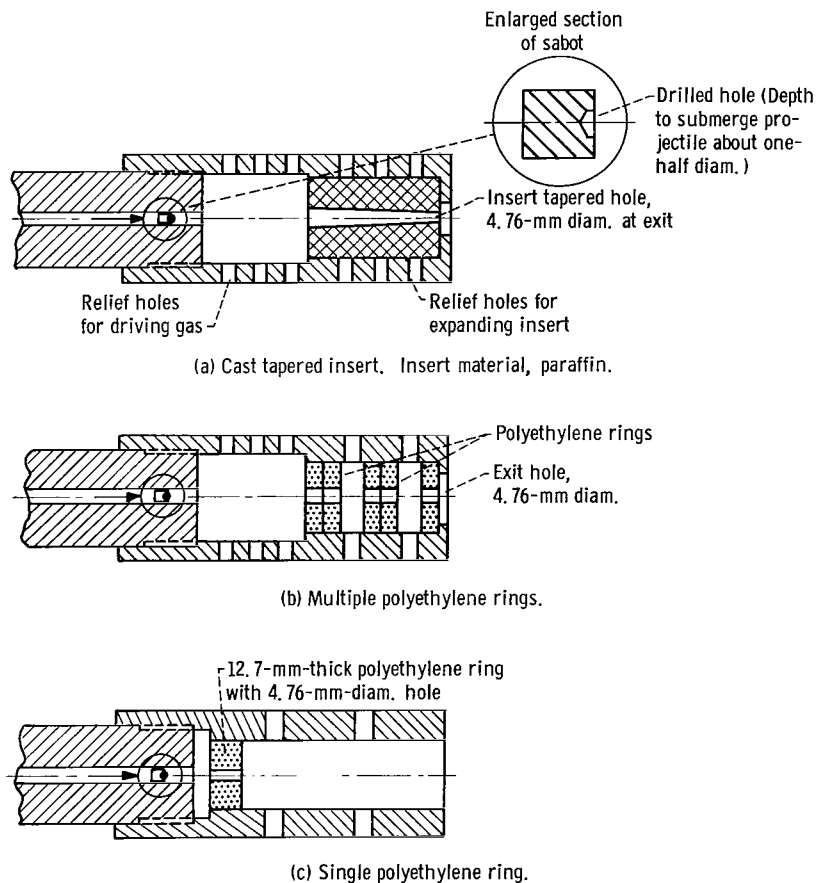with 4.76-mm-diam. hole

(c) Single polyethylene ring.

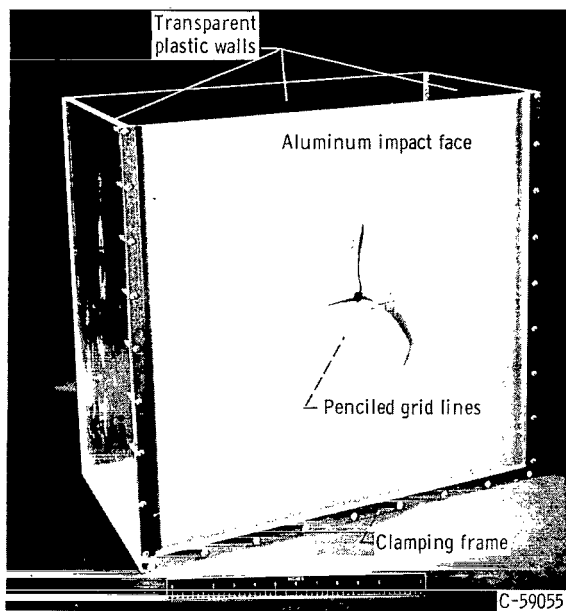Figure 3. - Sabot-projectile separating devices.

Figure 4. - Transparent plastic tank with impacted front wall of 0.794-millimeter-thick 7075-T6 aluminum.

holes of the prepunched walls were covered with either masking tape or a thin plastic film to allow the tanks to be filled with water above the level of the prepunched hole.

Instrumentation

Projectile velocity measurement. - Velocity measurements for projectiles accelerated by the 220 Swift rifle were obtained through the use of two capacitor type sensors located 30.5 centimeters (12 in.) apart (fig. 1, p. 3) and connected in a circuit with an electronic event timer. The sensors consisted of a Mylar sheet 6.35 microns (0.25 mil) thick coated with vapor deposited aluminum film on each side. A potential of 300 volts was applied across the Mylar film, and penetration of the sensor resulted in the shorting of the two layers of aluminum, which in turn discharged a capacitor and activated an electronic timer. The successive discharge pulses from the penetration of the two sensors were used to start, then stop, the electronic timer. Projectile velocities were calculated from the known distance separating the sensors and the projectile time of flight between the sensors.

For three data points where projectile velocities were not measured (due to electronic difficulties), approximate projectile velocities were determined from calibration curves previously established for this rifle through the use of the velocity measuring equipment. These curves were the result of numerous test shots made with projectiles of various materials and sizes and with varying amounts of powder in the rifle cartridge.

The velocity measurements for the projectiles accelerated by the light-gas gun were obtained through the use of a two-station projectile-detector system (fig. 5). This system consisted essentially of a mercury-vapor light source, a photoelectric detector at each station, and an electronic timer for recording the time of flight between the two stations. At each station, a screen of light was projected across the test section in a multiple-reflection fashion to cover the entire cross section. The reflecting beam of light finally impinged on a photoelectric detector. When the light screen at the first station was interrupted by the projectile, a change in the amount of light reaching the photoelectric cell was detected and a signal resulted which activated an electronic timer. The detection of the projectile at the second station stopped the electronic timer. Projectile velocities were then determined from the known distance and time of flight between the detector stations.
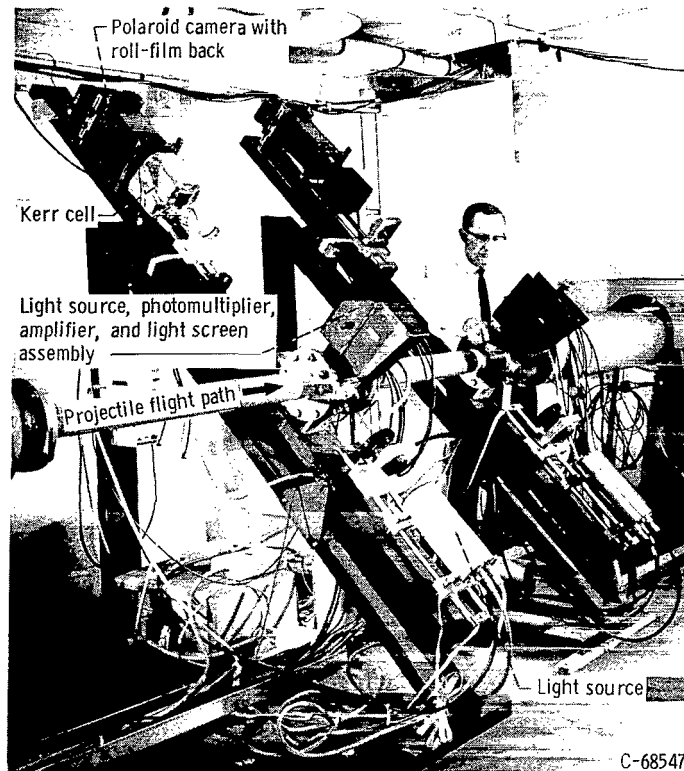
Figure 5. - Equipment for detecting and photographing projectile in flight and for providing an output for measurement of projectile velocity.

A Kerr Cell Shadowgraph system was used to obtain a short exposure (50 nsec) photograph of the projectile in flight. It consisted primarily of a light pulse generator, a Kerr Cell Shutter, and a camera, which were used in conjunction with each of the two stations of the projectile-detector system. The light pulse generator is activated simultaneously with the detector system as the projectile interrupts the light screen at each station. The Kerr Cell Shutter is synchronized with the light pulse generator to "open" or activate at the peak intensity of the light produced. An image of the object interrupting the light screen is thus exposed on the film plane of the camera to produce a shadowgraph. The shadowgraph serves to clearly identify and verify the integrity of the projectile.

High-Speed framing camera. - A high-speed, continuous-writing framing camera was used to evaluate visually and to analyze the progress of the pressure wave front as viewed through the sides of the water-filled plastic tanks. The camera is capable of taking 80 separate and sequential exposures spaced at equal time intervals. Framing rates up to 500 000 frames per second were used for this investigation. Figure 6 shows schematic diagrams of the two methods employed. The first method (fig. 6(a)) used direct illumination of the tank by directing a light beam through a collimating lens. The light rays were then directed through the sidewalls of the water-filled plastic tank and reflected by a mirror to the optical system of the framing camera. The shadowgraphs obtained with this method clearly define the pressure wave front and its propagation. The progress of the impacting projectile, however, was somewhat

8
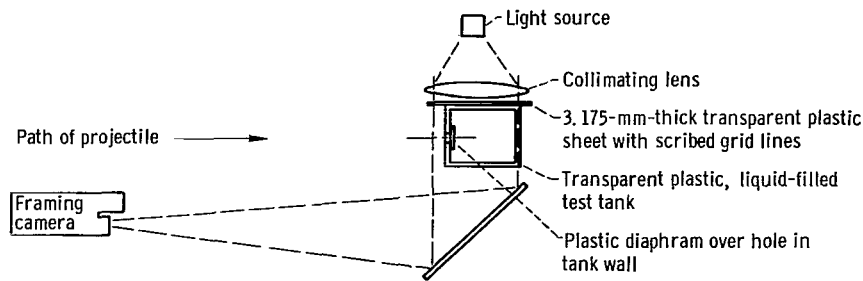
(a) Direct light rays.
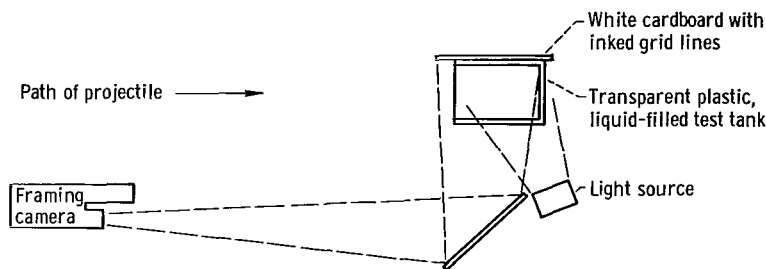
(b) Light reflected from grid board.

Figure 6. - Apparatus for photographing progress of impacting projectile and pressure wave front generated in liquid.

obscured by the shock front particularly at early times after impact. This prevented the accurate measurement of the progress of the projectile.

The second method (illustrated in fig. 6(b)) involved indirect illumination of the tank. A light source was directed on a white opaque background (with scribed grid lines) attached to the far sidewall of the tank; the light was then reflected back through the tank and directed to the camera through a mirror system. This method resulted in clear photographs of the movement of the projectile, but the shock front was not as clearly defined as in the method which produced the shadowgraphs. The progress of the shock front and/or the movement of the projectile was obtained by observing the individual frames of the photographs taken by the high-speed camera. Velocities for the shock front and the projectile were determined from the slopes of plotted curves showing the progress of the shock wave front or projectile with time. Pressures generated in the water corresponding to the measured shock front velocities were determined from data given in reference 8 which appears as figure 7 in this report. The value of the acoustic velocity in water used in reference 8 and in this investigation was 1.465 kilometers per second.

RESULTS AND DISCUSSION

This investigation was conducted primarily to analyze the characteristics of the pressure pulse generated in water from impact by a small high-velocity projectile and to measure the progress and energy loss of the projectile in the

Pressure at shock front, lbs/sq in.

Pressure at shock front, GN/m^2

.7x10^6

5.0
4.5
4.0
3.5
3.0
2.5
2.0
1.5
1.0
.5
0

Shock front velocity, km/sec
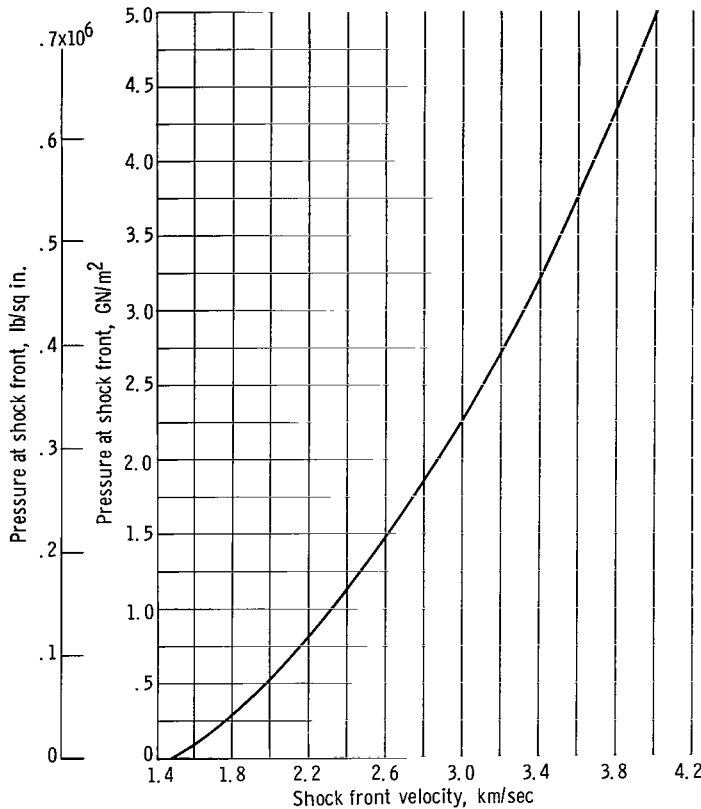1.4   1.8   2.2   2.6   3.0   3.4   3.8   4.2

Figure 7. - Shock front pressures as function of shock front velocity for water at 20° C. (Data taken from ref. 8.)

water. The characteristics of the pressure pulse are the shape and progress of the pressure wave front with time and the magnitude and decay characteristics of the pressure wave front.
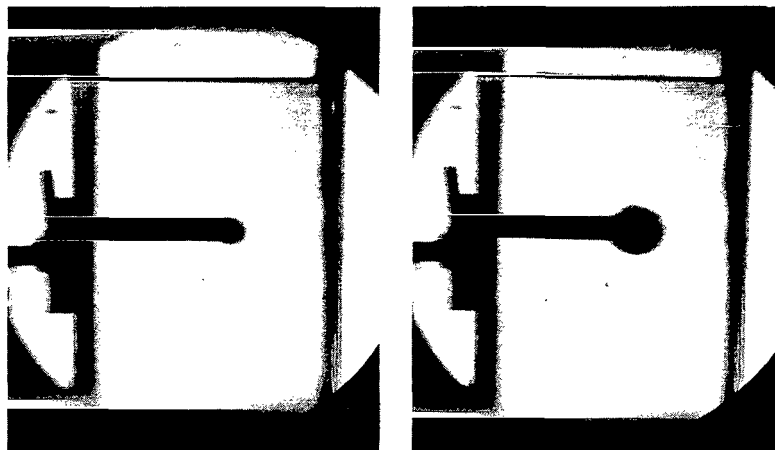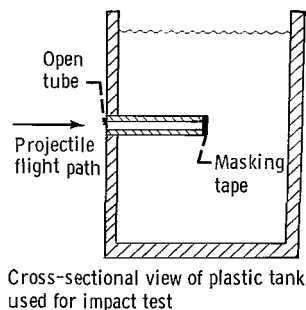
A summary of the tests conducted, together with a description of the projectiles and their impact conditions into water filled tanks, is presented in table I (p. 5).

Shape of Pressure Wave Front

The investigation of reference 1 indicated that the shape of the pressure wave front generated in water by a projectile impact was hemispherical with the point of impact as the origin. The data of the reference were limited, however, to impacts with spherical projectiles of a single diameter, and to impact Mach numbers (ratio of projectile impact velocity to the acoust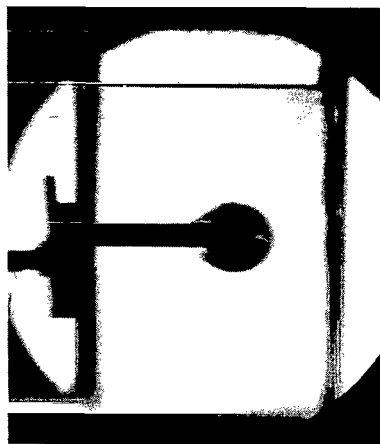ic-velocity of the liquid) into the liquid of less than 1.6. Since meteoroids have no fixed shape or composition and can travel at high velocities, the influence of several projectile materials, shapes, sizes, and velocities were investigated. This investigation used cylindrical and spherical projectiles 1.59 to 5.56 millimeters (1/16 to 7/32 in.) in diameter of several materials at impact Mach numbers as high as 4.37.

The shape and propagation of the resulting pressure wave front were obtained from observations of the high-speed shadowgraphs. Three typical shadowgraph sequences of the pressure wave front progress are shown in figures 8, 9, and 10. Figure 8 illustrates the results of impact by an aluminum sphere 5.56 millimeters (7/32 in.) in diameter at a velocity of approximately 1.89 kilometers per second into water in a transparent plastic tank (test number 1, table I). The tank had a tube extending into the center of the liquid, through which the projectile traveled to impact into the liquid at the center of the tank. A schematic of the tank is also shown in figure 8. A piece of masking tape was used to cover the tube end at the center of the tank to contain the water. The purpose of the impact was to demonstrate that a spherical wave front would result from an impulsive transfer of the energy of the projectile into the water. The photographs in figure 8 indicate that a spherical wave front is indeed generated and that the center of the spherical surface remains at the point of impact with time after impact. These results indicated that there was no significant effect of the forward momentum of the projectile to move the wave front

10

Open tube ⌐
Projectile flight path
Masking tape

Cross-sectional view of plastic tank used for impact test

4   12
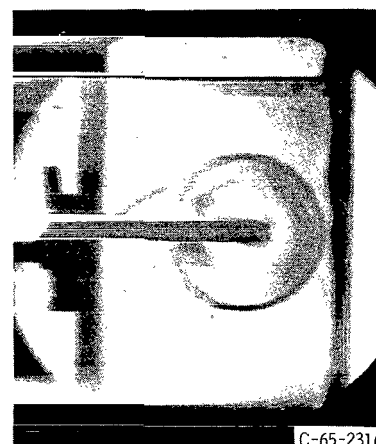
20   39   51

C-65-2316

Time after impact, μ sec

Figure 8. - Progress of pressure wave generated in water by impact at tank center. Projectile, 5.56-millimeter-diameter aluminum sphere; velocity, 1.89 kilometers per second; test 1.

in the direction of flight. The results of projectile impact thus can be compared to a point source energy release.

The results of a 3.175-millimeter-diameter (1/8 in. diam.) steel sphere impacting obliquely into the metal front wall of a tank at a velocity of 2.64 kilometers per second (test number 2, table I) are shown in figure 9. The shadowgraphs of the expanding pressure front indicate no observable effect of the momentum or flight direction of the projectile (i.e., a hemispherical wave front was produced and the center of the hemisphere remained at the point of impact as the wave front expanded). The other wave front in the water, which appears as a straight line oblique to the metal wall (fig. 9) or to the plastic tube (fig. 8), was caused by the movement of a pressure wave through the metal or plastic at a faster rate than through the water.
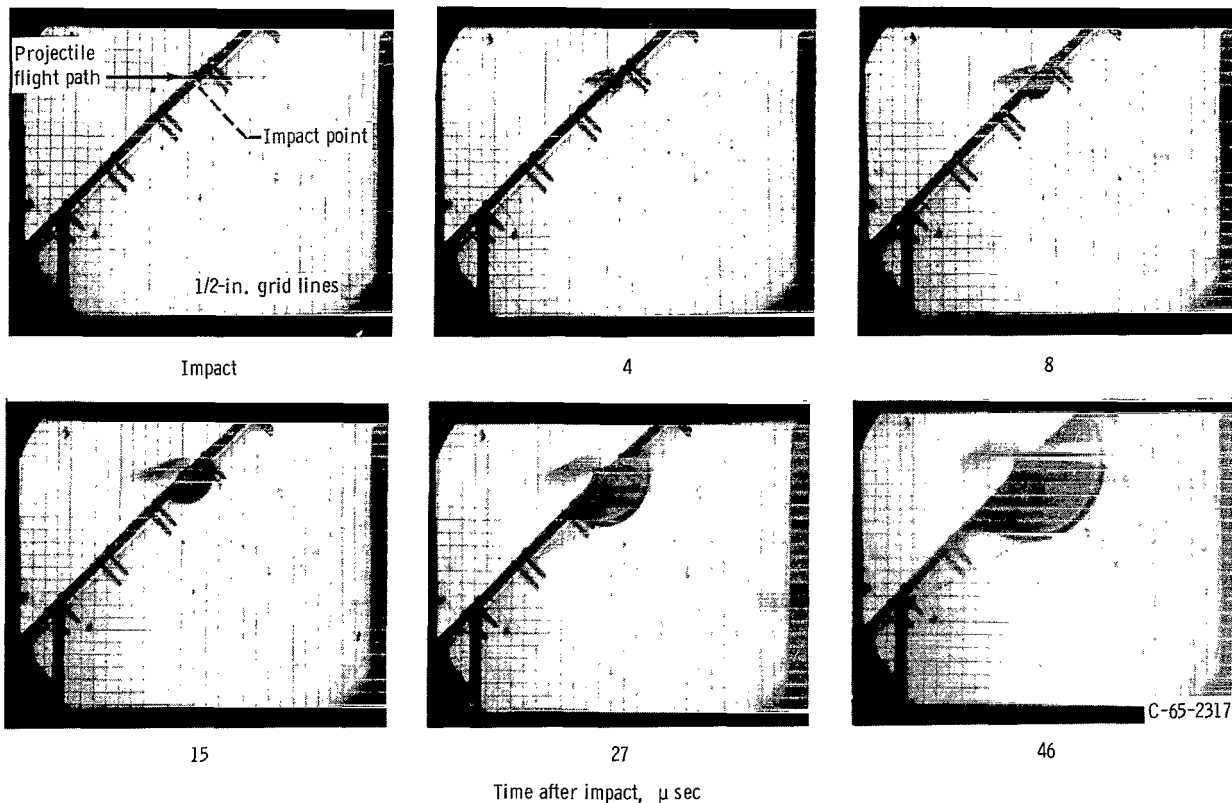
Figure 9. - Progress of pressure wave generated in water by oblique impact into tank wall. Projectile, 3.175-millimeter-diameter steel sphere; velocity, 2.64 kilometers per second; test 2.

Figure 10 shows shadowgraphs of an impact by a 1.59-millimeter-diameter (1/16 in. diam.) steel sphere at a velocity of 5.35 kilometers per second (test no. 3) directly into the water through a thin plastic sheet which covered a prepunched hole in the front tank wall. The figure indicates the same hemispherical growth of the pressure wave front about the impact point as shown in figures 8 and 9. Figure 10 also shows the breakup of this high-velocity projectile after impact. The movement of fragments of the broken projectile can be seen in the figure.

The results of these tests and the others listed in table I indicated that the pressure wave front was essentially hemispherical and remained hemispherical regardless of the condition of impact: that is, projectile size, shape, material, velocity, orientation, and condition of wall (solid or prepunched). The origin or center of the hemispherical surface also remained fixed at the impact point. Thus, the assumption of a hemispherical wave front used in the analysis of wave front progress in solids (refs. 2 to 4) can also be applied to impacts into water.

Progress of Wave Front With Time

Impacts with projectiles of various sizes and materials at velocities as high as 6.4 kilometers per second were made to determine the progress of the

12
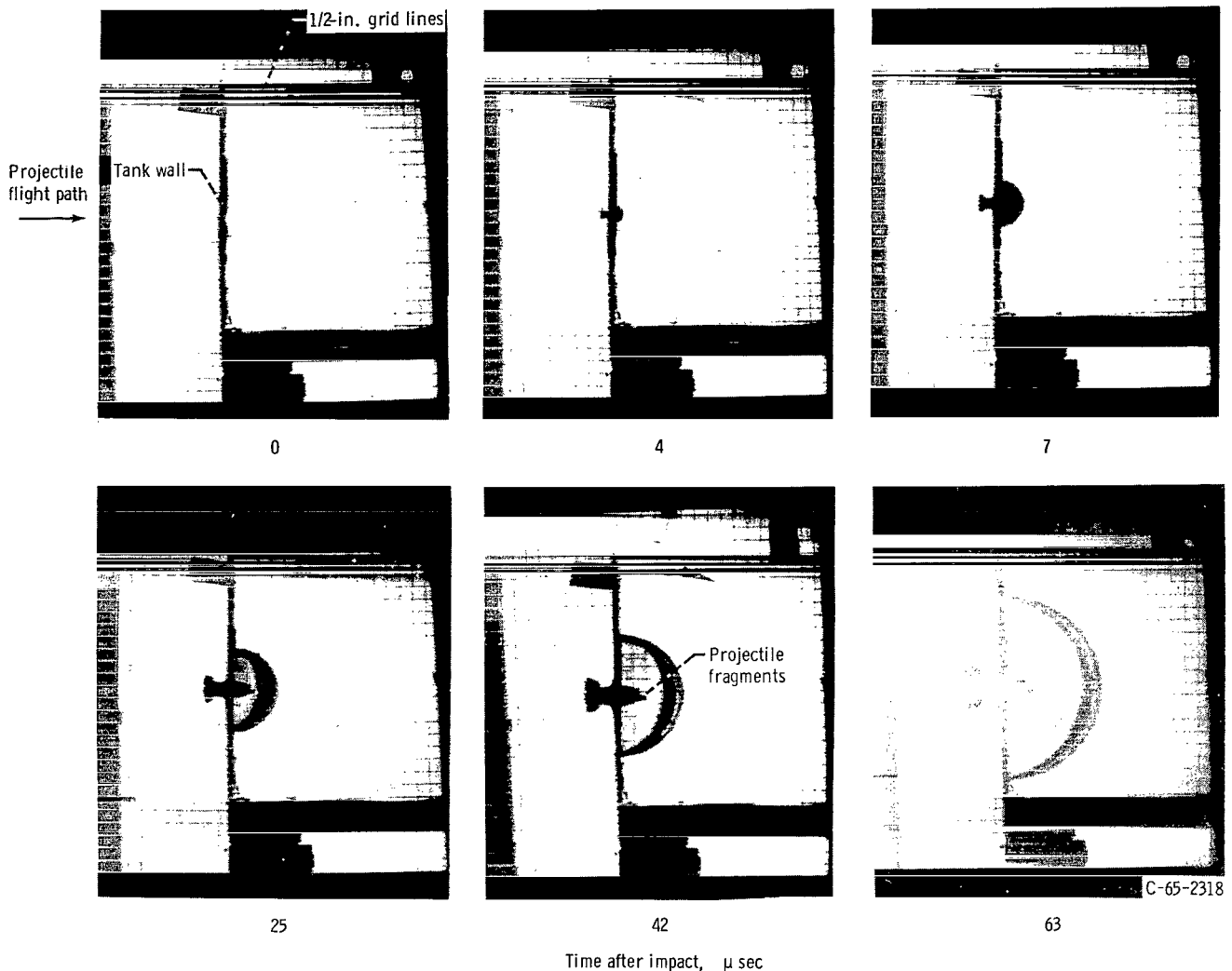
Figure 10. – Shadowgraphs of pressure wave produced by impact through prepunched hole into water-filled tank. Projectile, 1.59-millimeter-diameter steel sphere; velocity, 5.35 kilometers per second; test 3.

wave front with time. The wave front progress was determined from shadowgraphs (similar to those in fig. 10) taken at approximately 2 or 4 microsecond intervals. Some typical results are plotted in figure 11. The wave front progress with time for all impact tests, obtained from curves such as figure 11, is summarized in table II. In general, the data indicate that the progress of the wave front was proportional to time to about the 0.8 power, the exponents ranging from 0.7 to 0.9.

In order to determine whether the measured progress of the wave front in water was related to that obtained from impacts into solids the data were compared in figure 12 to the experimental results from references 9, 10, and 11. The targets of these references were Lucite and wax, which were impacted by high-velocity steel, aluminum, and plastic projectiles. The data indicate that the progress of the wave front in the solids was also proportional to time to about the 0.8 power.

13

TABLE II. - PROGRESS OF THE SHOCK FRONT GENERATED IN WATER BY PROJECTILE IMPACT

Test number	Projectile				Shock front radius, cm								
	Diameter, mm	Shape	Material	Velocity, km/sec	Time after impact, μsec								
					2	4	6	8	10	20	30	50	70
Impact into water through prepunched hole													
3	1.59	Sphere	Steel	5.35	----	0.77	1.16	1.55	1.90	3.60	5.05	7.75	-----
4	3.175	Sphere	Aluminum	5.27	----	.89	1.34	1.75	2.18	3.85	5.33	8.10	-----
5	5.56	Sphere	Aluminum	2.32	----	1.18	1.63	2.06	2.46	4.25	5.90	8.90	-----
6	5.56	Cylinder	Copper	3.96	----	1.60	2.20	2.75	3.25	5.40	7.30	10.50	-----
7	5.56	Cylinder	Steel	4.27	1.09	1.83	2.49	3.07	3.61	5.92	7.75	11.18	-----
8	3.175	Sphere	Steel	4.27	----	1.02	1.45	1.88	2.26	4.06	5.51	8.69	-----
9	5.56	Sphere	Aluminum	1.90	----	----	2.06	2.39	2.72	4.39	6.10	9.40	12.45
10	5.56	Sphere	Tungsten carbide	~1.80	----	1.65	2.08	2.46	2.84	4.62	6.35	-----	-----
11	5.56	Cylinder	Copper	~1.31	----	1.02	1.40	1.75	2.11	3.73	5.33	8.38	11.30
16	5.56	Sphere	Steel	1.87	.31	.66	1.02	1.37	1.73	3.43	5.08	-----	-----
17	5.56	Sphere	Aluminum	1.67	----	----	----	1.50	1.83	3.38	4.95	7.70	10.67
Impact into tank wall before impact into water													
12	5.56	Sphere	Aluminum	~1.83	----	1.70	2.16	2.59	2.97	4.88	6.73	10.16	13.46
13	3.175	Sphere	Steel	3.75	----	----	1.37	1.80	2.24	4.14	5.84	-----	-----
14	3.175	Sphere	Steel	3.20	----	----	1.27	1.70	2.11	4.06	5.92	9.27	-----
15	5.56	Cylinder	Nylon	6.40	----	----	1.68	2.11	2.52	4.47	6.25	9.53	12.57

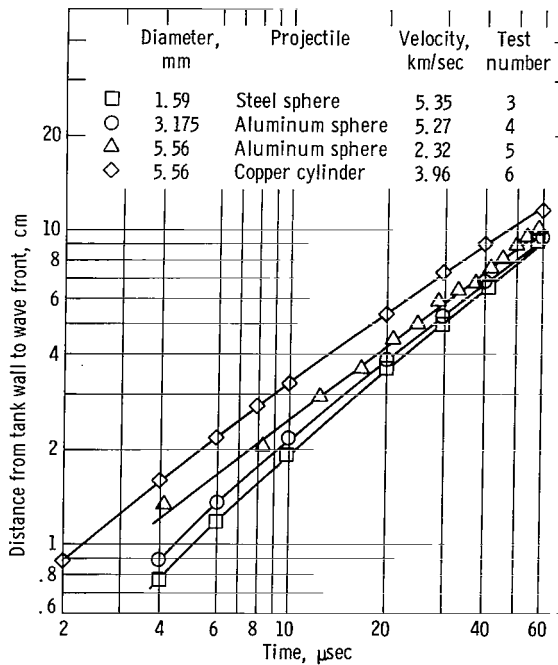|	Diameter, mm	Projectile	Velocity, km/sec	Test number
□	1.59	Steel sphere	5.35	3
○	3.175	Aluminum sphere	5.27	4
△	5.56	Aluminum sphere	2.32	5
◇	5.56	Copper cylinder	3.96	6

Figure 11. - Progress of typical pressure wave front in water with time generated by projectile impact.
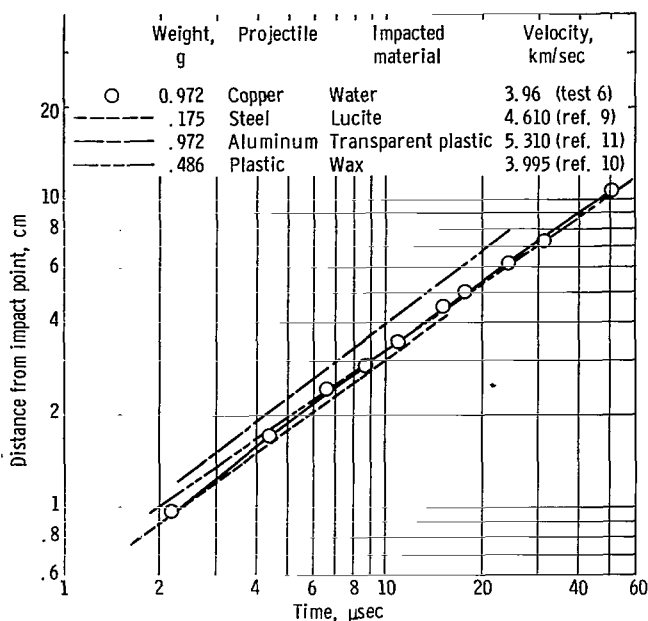
Figure 12. - Comparison of progress of pressure wave fronts generated by impacts into several materials.

Weight, g	Projectile	Impacted material	Velocity, km/sec
O 0.972	Copper	Water	3.96 (test 6)
----- .175	Steel	Lucite	4.610 (ref. 9)
----- .972	Aluminum	Transparent plastic	5.310 (ref. 11)
----- .486	Plastic	Wax	3.995 (ref. 10)

This relation, however, does not determine the magnitudes of the radii or the velocities of shock front. The analytical methods of references 4 and 6 were employed for this purpose. The shock wave front radius in a given media was predicted in reference 4 to be a function of the projectile impact kinetic energy, shock wave front velocity, and time. The shock wave front radius in reference 6 was indicated to be a function of time, projectile impact kinetic energy, and projectile size. The method presented in reference 4 was an analytical derivation of equations of wave front radius while that of reference 6 was a semiempirical approach.

The wave front radius and its rate of change predicted by the method of reference 4 agreed well with experimental data of impacts with projectiles of high impact energy. The data, however, showed progressively greater disagreement with predictions as projectile impact energy or diameter were decreased.

The predictions of wave front radius with time using the equation of reference 6 which considered the effect of projectile size showed poor correlation with the experimental data; however, when the semiempirical equation in reference 6 which correlated the experimental data of constant diameter projectiles was used and assumed to apply to all sizes of projectiles, good agreement with the data was obtained. In general the equation, containing only the projectile energy and time, predicted the location of the shock wave front at any time within 0.254 centimeter (0.1 in.) of that experimentally obtained for all sizes of projectiles investigated. The results obtained indicate that the wave front radius and its velocity in water, in general, are proportional to the kinetic energy of the projectile and are not significantly influenced by the separate effects of projectile size, shape, material, or velocity.

Pressures Generated at Wave Front

The pressures generated in water at the wave front were determined by using the relation of wave front velocity to pressure shown in figure 7 (p. 10) which was obtained from data presented in reference 8. The velocities of the wave fronts were determined from the slopes of curves of the wave front progress with time from the shadowgraphs. The pressures generated at the shock front for a number of impact conditions is shown in figure 13 plotted against distance from the impact point. The results show that extremely high pressures are generated in the water near the point of impact. For example, impact with a
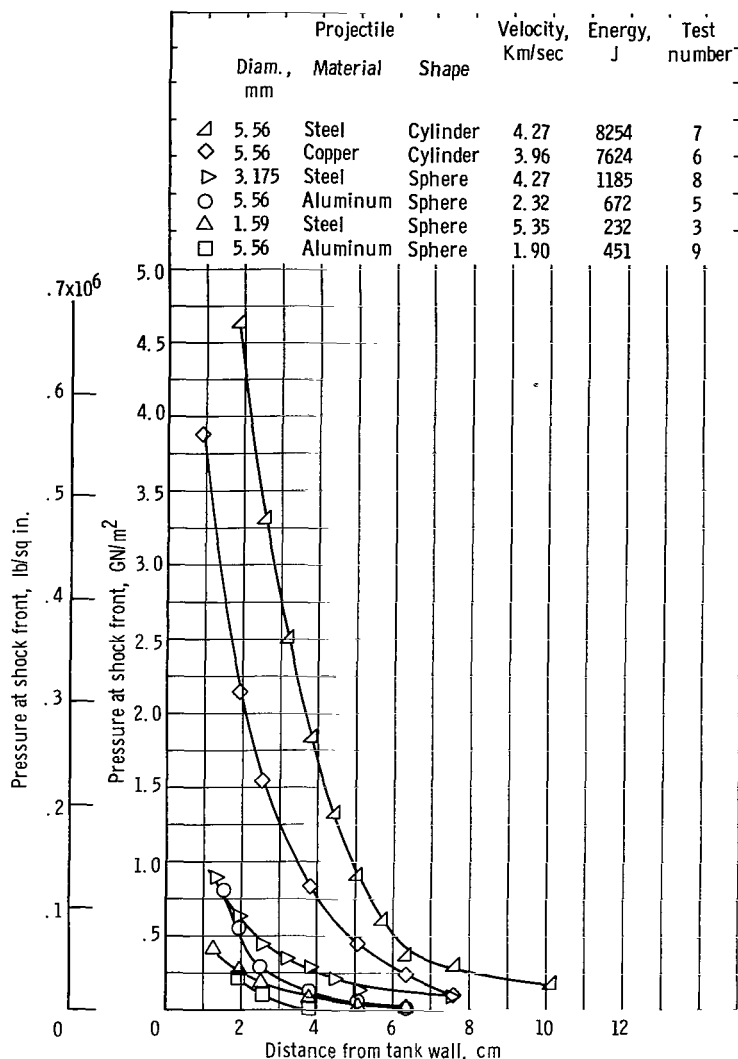
15

	Projectile			Velocity, Km/sec	Energy, J	Test number
	Diam., mm	Material	Shape			
⊿	5.56	Steel	Cylinder	4.27	8254	7
◇	5.56	Copper	Cylinder	3.96	7624	6
▷	3.175	Steel	Sphere	4.27	1185	8
○	5.56	Aluminum	Sphere	2.32	672	5
△	1.59	Steel	Sphere	5.35	232	3
□	5.56	Aluminum	Sphere	1.90	451	9

Pressure at shock front, lb/sq in.

Pressure at shock front, GN/m²

Distance from tank wall, cm

Figure 13. – Shock front pressures generated in water by impact with high-velocity projectiles.

5.56-millimeter (7/32 in.) steel cylinder (length-to-diameter ratio of 1) at an impact velocity of 4.27 kilometers per second (test no. 7) resulted in pressures as high as 4.63 giga newtons per square meter (0.67×10^6 lb/sq in.) at distance of 1.9 centimeters (3/4 in.) from the impact point. This is about the nearest distance from the tank wall or impact point that an accurate measurement of the wave front velocity could be obtained for pressure calculations. These pressures at the front decayed rapidly, however, even for the projectiles with high impact energies and approached ambient values within about 13 centimeters (5 in.) from the impact point, generally less than 70 microseconds after projectile impact. These results would indicate that even for impacts with high-velocity and high kinetic energy projectiles the side or rear walls of a tank 13 centimeters (5 in.) or more from the impact point would not be subjected to a significant pressure pulse.

16

Figure 14. – Progress of projectiles with time after impact into water.

The figure contains the following legend:

Impacts into water through prepunched hole in tank

	Diameter, mm	Projectile	Velocity, km/sec	Test number
O	5.56	Aluminum sphere	2.32	5
□	5.56	Tungsten carbide sphere	~1.80	10
◇	5.56	Copper cylinder	~1.31	11
▽	3.175	Aluminum sphere	5.27	4
◁	1.59	Steel sphere	5.35	3

Impacts into solid tank wall

	Diameter, mm	Projectile	Velocity, km/sec	Test number
△	5.56	Aluminum sphere	~1.83	12
◺	3.175	Steel sphere	3.75	13

Decay of Projectile Velocity After Impact Into Water

Measurements were made of the progress of the projectile in water after impact by using the shadow-graphs. From these measurements the projectile velocity and energy loss were determined.

The projectile progress in water for a variety of impact conditions is shown in figure 14. The distance from the point of impact that the projectile or the foremost projectile fragments traveled is plotted against time after impact. For impact velocities less than about 2.4 kilometers per second, obtained with the high-speed rifle, the projectiles generally deformed but remained intact throughout the penetrating process.

The data plotted in figure 14 indicates that the aluminum sphere (test 5) decelerated at a faster rate than did the more massive tungsten sphere (test 10) and also that the heavy long copper cylinder with a length-to-diameter ratio of about 2.7 (test 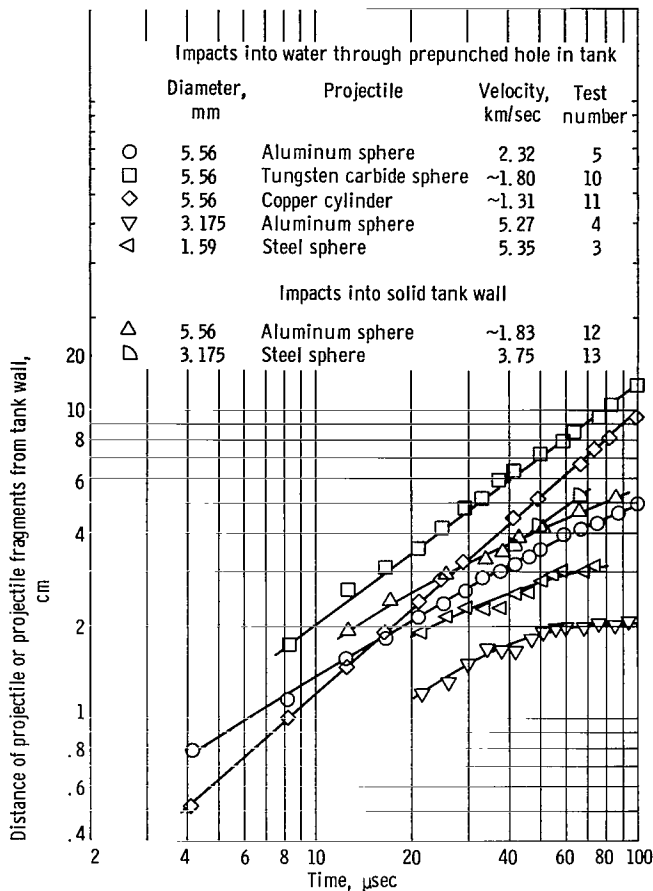11) was not appreciably slowed down during the period in which measurements were obtained. At the higher impact velocities (5.27 and 5.35 km/sec) the slopes of the data in figure 14 indicate that these projectiles decelerated more rapidly than the low-velocity projectiles (1.31 to 3.75 km/sec). One of the projectiles, the 3.175-millimeter-diameter (1/8 in.) aluminum sphere at an impact velocity of 5.27 kilometers per second (test 4), for example, was essentially stopped 2 centimeters from the impact point or in about 80 microseconds after impact. The breakup of the projectiles that was observed in the water for the higher impact velocities would result in a higher drag and more rapid deceleration of these projectiles.

Projectile Energy Loss Data and Comparison with Predictions

The experimentally obtained ratio of the energy of the impacting projectile at any time after impact to the initial impact kinetic energy for a variety of projectile sizes, velocities, and several materials is shown in figure 15. The impacts with the 1.59-millimeter-diameter (1/16 in. diam.) steel and 3.175-millimeter-diameter (1/8 in. diam.) aluminum projectiles at velocities above 5.2 kilometers per second (tests 3 and 4, for example) result in trans-
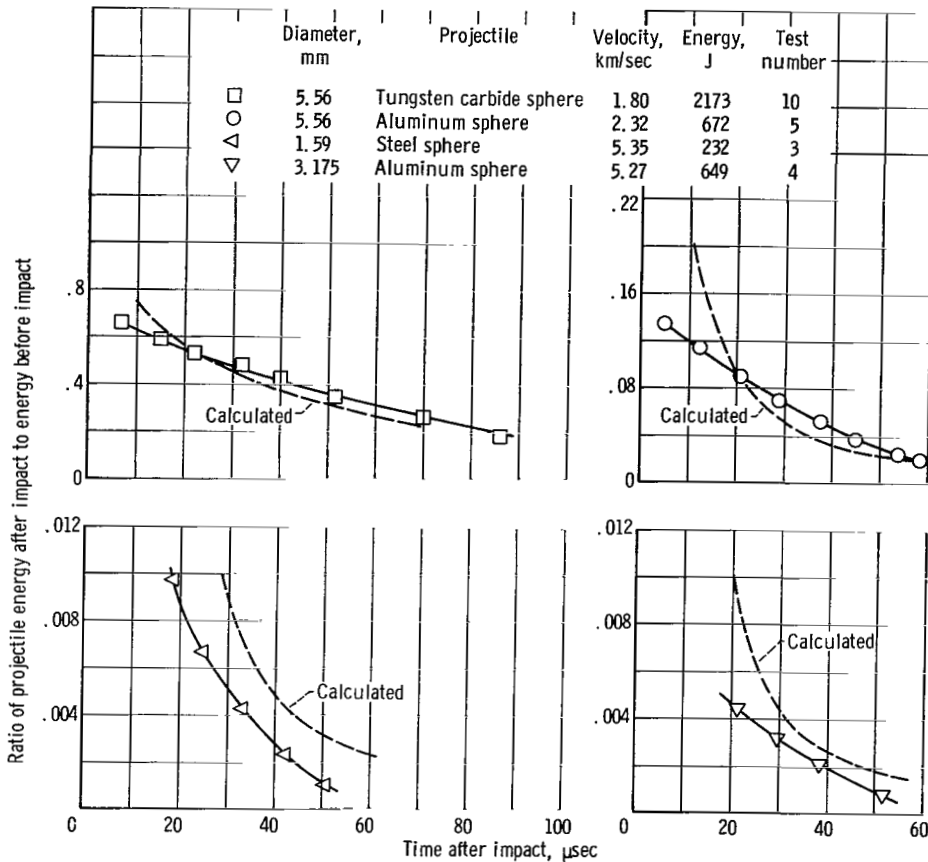
17

Figure 15. - Experimental and calculated ratios of projectile energies after impact into water to energies before impact.

ferring about 99 percent of the initial impact energy to the water in only 20 microseconds after impact. Thus, the projectile energies are rapidly lost after impact and transferred to the liquid, particularly for the smaller high-velocity projectiles. Data from the figure also indicate that although the initial impact kinetic energies varied by a factor of 9.3 (test 10 compared with test 3) the amount of energy transferred to the water 20 microseconds after impact differed by a factor of only about 4.3.

These observations may indicate that for the same impact kinetic energies, a more damaging pressure pulse for wall fracture may result from impact by small high-velocity projectiles than with more massive low-velocity projectiles. The total energy deposited in the liquid and transferred to the tank wall at short times after impact would be expected to be greater for the small high-velocity projectile although the pressure at the wave fronts would be expected to be the same based on prior results which indicated that the wave front velocity was a function of the projectile impact kinetic energy.

A shock interaction process between the projectile and the impacted liquid governs the velocity of the shock front and the pressure at the shock front. However, the viscous deceleration of the projectile and the energy deposited in the liquid with time, particularly for the more massive, lower velocity projec-

tiles, influences the characteristics of the pressure pulse behind the shock front. The data of reference 1 indicate that the viscous deceleration of the projectile may influence the initiation of the wall fracture and would certainly influence the extension of the initiated cracks because the data (ref. 1) indicate that the time for initiation of wall fracture ranged from 27 to 40 microseconds after impact and that the extension of the crack continued for several hundred microseconds. Thus any energy transferred to the liquid during this time could influence the pressure pulse felt by the wall.

A rigorous analysis of the velocity decay or energy loss of a projectile after it impacts and progresses through a water filled tank would be extremely difficult because of the unknowns. Reasonable assumptions are difficult to make for effects such as the change in shape or fragmentation of the projectile with time and the interrelation of these factors with the projectile material properties. Because of these difficulties a simplified analysis of the projectile energy loss was made and compared with experimental data. This analysis employed a simple drag equation and considered the deceleration of spherical projectiles in water assuming a drag coefficient of 1.0 for the projectile. It was also assumed that the projectile remained intact and did not deform.

The following equation was used:

$$D = - m \frac{dV}{dt} = C_D A_P \rho L \frac{V^2}{2g}$$

Rearranging terms, integrating, solving for the velocity V for spherical projectiles, and then dividing the equation through by the impact velocity V_o give the projectile velocity decay ratio:

$$\frac{V}{V_o} = \frac{1}{1 + \frac{3}{4} C_D \left(\frac{\rho_L V_o}{\rho_P d_P}\right) t} \tag{2}$$

Squaring both sides of this relation then gives the ratio of the projectile energy after impact to the projectile impact energy:

$$E_R = \frac{1}{\left[1 + \frac{3}{4} C_D \left(\frac{\rho_L V_o}{\rho_P d_P}\right) t\right]^2} \tag{3}$$

where

D   drag force

m   projectile mass

V   projectile velocity

t   time after impact

C_D drag coefficient

A_p projectile cross-sectional area

ρ_L liquid density

g   gravitational constant

V_o projectile impact velocity

E_R ratio of projectile energy after impact to initial impact energy

d_p projectile diameter

ρ_p projectile density

The results of the calculations are compared to the experimentally obtained data in figure 15. The comparison indicates that in spite of the simplifying assumptions the agreement between the calculated and experimental values of the ratios of the projectile energy after impact to initial impact energy was reasonably good. The actual projectile energy lost at early times after impact was generally greater than that predicted but tended to agree at longer times.
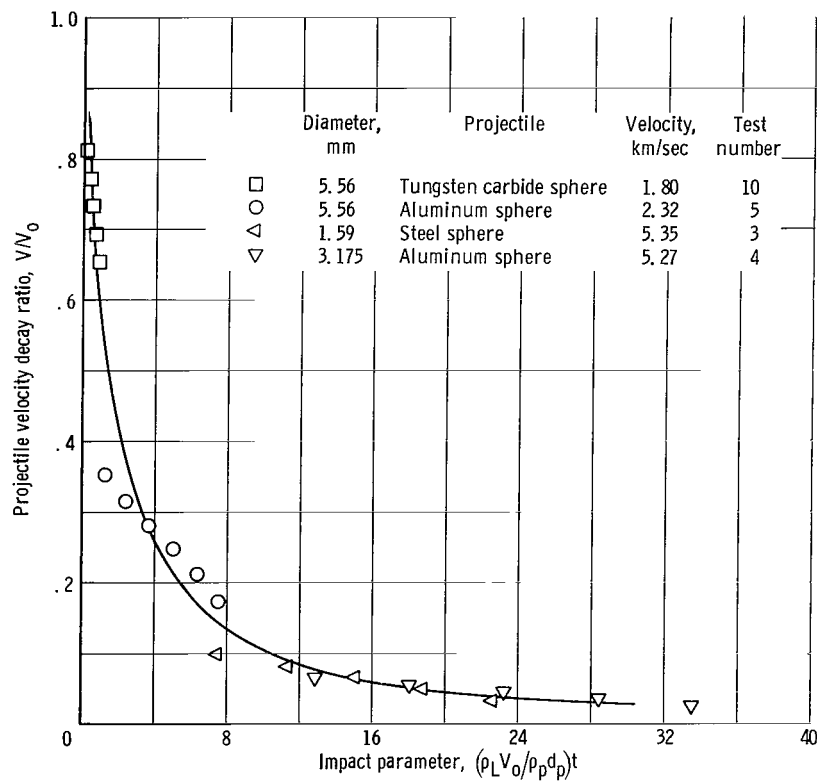

	Diameter, mm	Projectile	Velocity, km/sec	Test number
□	5.56	Tungsten carbide sphere	1.80	10
○	5.56	Aluminum sphere	2.32	5
◁	1.59	Steel sphere	5.35	3
▽	3.175	Aluminum sphere	5.27	4

Projectile velocity decay ratio, V/V_0

Impact parameter, $(\rho_L V_0/\rho_p d_p)t$

Figure 16. – Projectile velocity decay ratio against impact parameter.

In attempting to provide a method for predicting the projectile energy decay with time, it was found that a plot of the experimental projectile velocity decay ratio V/V_O for spherical projectiles (tests 3, 4, 5, and 10) against the dimensionless impact parameter $(\rho_L V_O/\rho_P d_P)t$ resulted in a curve shown in figure 16. Considering that a single curve approximates the results of a wide range of projectile impact conditions, suggests that the curve can also be used to predict the velocity (or energy) decay for projectiles with specified values of this impact parameter. The shape of the curve in figure 16 indicates rapid decays in projectile velocity (or energy) for large values of the impact parameter. The terms in the parameter further indicate that rapid decays in the projectile velocity will occur for projectiles with high impact velocities, low densities, and small diameters.

The complex nature of the impact, deceleration, deformation, and fragmentation of projectiles dictates that care should be exercised in using the curve particularly beyond the conditions of the experimental data.

SUMMARY OF RESULTS

The following results and conclusions were obtained from the investigation of the characteristics of pressure waves generated in water as a result of impacts by high velocity projectiles of various materials and sizes:

1. The energy of the impacting projectile is rapidly transferred to the liquid. At any given time after impact, the small, high velocity projectiles lost a larger part of their impacting kinetic energy than did the more massive, lower velocity projectiles. This observation may indicate that for the same impact kinetic energies, a more damaging pressure pulse for wall fracture may result from impact by small high velocity projectiles than with more massive low velocity projectiles.

2. Analytical predictions of the energy lost by spherical projectiles with time after impact, considering only drag forces on the projectile, agreed well with experimental data.

3. The rapid energy transfer produces essentially a "point source" energy release resulting in a hemispherically shaped pressure wave front emanating from the point of impact. The hemispherical shape of the front was found to exist for normal and oblique impacts and in addition was found to be insensitive to whether impacts were made into thin solid metal or directly into water through prepunched tank walls.

4. The progress of the pressure wave front during the period of intense pressures in the water was found to be proportional to time to an exponent of about 0.8. Approximately the same progress of the wave front was obtained, by others, when solids (wax and plastic) were impacted by high velocity projectiles.

5. Extremely high pressures were generated in the liquid as a result of the impact. Impact by a 5.56-millimeter-diameter (7/32-in. diam) steel cylinder at a velocity of 4.27 kilometers per second resulted in pressures as

high as 4.63 giga newtons per square meter (0.67×10^6 psi) at a distance of 1.9 centimeters (3/4 in.) from the point of impact. The pressure at the wave front decayed rapidly, and approached ambient values within about 13 centimeters (5 in.) from the impact point or within about 70 microseconds after impact.

Lewis Research Center,
    National Aeronautics and Space Administration,
        Cleveland, Ohio, August 10, 1965.

REFERENCES

1. Stepka, Francis S.; and Morse, C. Robert: Preliminary Investigation of Catastrophic Fracture of Liquid-Filled Tanks Impacted by High-Velocity Particles. NASA TN D-1537, 1963.

2. Davids, Norman; and Huang, S. W.: Shock Wave Propagation in Crater Formation. Tech. Rept. No. 2, Penn State Univ., Dec. 31, 1960.

3. Rae, William J.: A Study of Meteroid Impact Phenomena. NASA CR-58058, 1962.

4. Rae, William J.; and Kirchner, Henry P.: A Blast-Wave Theory of Crater Formation in Semi-Infinite Targets. Proc. Sixth Symposium on Hypervelocity Impact, Vol. 2, Pt. 1, Aug. 1963, pp. 163-227.

5. Heyda, James F.: Shock Front Variation in Time for High Impact into Water. Proc. Sixth Symposium on Hypervelocity Impact, Vol. 2, Pt. 1, Aug. 1963, pp. 321-336.

6. Chou, Pei Chi; Sidhu, Harbans S.; Karpp, Robert R.: Analysis of Peak Pressure Generated in Water by High Velocity Impact. NASA CR-50249, 1963.

7. Curtis, John S.: An Accelerated Reservoir Light-Gas Gun. NASA TN D-1144, 1962.

8. Cole, Robert H.: Underwater Explosions. Princeton Univ. Press, 1948, pp. 36-47.

9. Halperson, S. M.; and Hall, D. A.: Shock Studies in Transparent Plastic by High Speed Photographic Technique. Rept. of NRL Prog., Naval Res. Lab., Sept. 1961.

10. Frasier, J. T.; and Karpov, B. G.: Hypervelocity Impact Studies in Wax. Proc. Fifth Symposium on Hypervelocity Impact, Vol. I, Pt. 2, 1962, pp. 371-388.

11. Kineke, John H., Jr.: Observation of Crater Formation in Ductile Materials. Proc. Fifth Symposium on Hypervelocity Impact, Vol. 1, Pt. 2, 1962, pp. 339-370.

"The aeronautical and space activities of the United States shall be conducted so as to contribute . . . to the expansion of human knowledge of phenomena in the atmosphere and space. The Administration shall provide for the widest practicable and appropriate dissemination of information concerning its activities and the results thereof."

—NATIONAL AERONAUTICS AND SPACE ACT OF 1958

NASA SCIENTIFIC AND TECHNICAL PUBLICATIONS

TECHNICAL REPORTS: Scientific and technical information considered important, complete, and a lasting contribution to existing knowledge.

TECHNICAL NOTES: Information less broad in scope but nevertheless of importance as a contribution to existing knowledge.

TECHNICAL MEMORANDUMS: Information receiving limited distribution because of preliminary data, security classification, or other reasons.

CONTRACTOR REPORTS: Technical information generated in connection with a NASA contract or grant and released under NASA auspices.

TECHNICAL TRANSLATIONS: Information published in a foreign language considered to merit NASA distribution in English.

TECHNICAL REPRINTS: Information derived from NASA activities and initially published in the form of journal articles.

SPECIAL PUBLICATIONS: Information derived from or of value to NASA activities but not necessarily reporting the results of individual NASA-programmed scientific efforts. Publications include conference proceedings, monographs, data compilations, handbooks, sourcebooks, and special bibliographies.

Details on the availability of these publications may be obtained from:

SCIENTIFIC AND TECHNICAL INFORMATION DIVISION

NATIONAL AERONAUTICS AND SPACE ADMINISTRATION

Washington, D.C. 20546